Nucl. Phys. A 1053 (2025) 122967

Contents lists available at ScienceDirect

Nuclear Physics A

journal homepage: www.elsevier.com/locate/nuclphysa

Alpha spectroscopy of purified beams of exotic nuclei at the FRS Ion Catcher

Nazarena Tortorelli [a,c,*], Moritz Pascal Reiter [b,f], Ann Kathrin Rink [b], Sivaji Purushothaman [c], Samuel Ayet San Andrés [c], Julian Bergmann [b], Timo Dickel [c,b], Marcel Diwisch [b], Jens Ebert [b], Hans Geissel [c,b,1], Florian Greiner [b], Emma Haettner [c], Christine Hornung [b], Aleksandra Kelic-Heil [c], Ronja Knoebel [c], Wayne Lippert [b], Ivan Miskun [b], Iain D. Moore [d], Stephane Pietri [c], Wolfgang R. Plaß [c,b], Ilkka Pohjalainen [d], Andrej Prochazka [c], Christoph Scheidenberger [c,b,e], Maya Takechi [c], Peter G. Thirolf [a], Helmut Weick [c], John Winfield [c,1], Xiaodong Xu [c]

[a] *Ludwig-Maximilians-Universität München, 85748 Garching, Germany*
[b] *II. Physikalisches Institut, Justus-Liebig-Universität Gießen, 35392 Gießen, Germany*
[c] *GSI Helmholtzzentrum für Schwerionenforschung GmbH, 64291 Darmstadt, Germany*
[d] *University of Jyväskylä, 40014 Jyväskylä, Finland*
[e] *Helmholtz Research Academy Hesse for FAIR (HFHF), GSI Helmholtz Center for Heavy Ion Research, Campus Gießen, 35392 Gießen, Germany*
[f] *University of Edinburgh, United Kingdom*

ARTICLE INFO

Keywords:
FRS-IC
α-spectroscopy
Nuclear structure
Half-life

ABSTRACT

The FRS Ion Catcher (FRS-IC) is located at the final focal plane of the Fragment Separator FRS at GSI. The FRS-IC setup is well known for high-precision experiments with stopped exotic nuclei produced by projectile fragmentation and fission. The facility consists of the cryogenic gas-filled stopping cell (CSC), an RFQ-based beamline (DISTRICT), and a multiple-reflection time-of-flight mass spectrometer (MR-TOF-MS). This paper illustrates how alpha spectroscopy performed at this facility has emerged as a promising tool to unveil the nuclear structure of exotic nuclei, i.e., half-live and decay energy measurements. First studies of that kind were performed on the decay chains of ^{218}Rn, ^{219}Rn, ^{221}Ac, ^{220}Fr, and ^{223,224}Th produced by projectile fragmentation of ^{238}U. The α decay energy measurements performed and the deduced Q_α values confirm the known maximum at N= 128 and the values of Q_α at N= 132 – 133 follow the predicted increasing in Q_α values compared to the values for At isotopes at the same neutron number N. Further, the production rate ratio of the isomer to the ground state of ^{211}Po was measured. It allows an estimate of the angular momentum distribution of ^{211}Po fragments following fragmentation of ^{238}U in a ^{9}Be target at relativistic energies. In addition, the potential of mass-selected decay spectroscopy behind the MR-TOF-MS was demonstrated with short-lived ^{215}Po ions ($t_{1/2}$ = 1.78 ms). This demonstrates that the FRS-IC is a reliable setup for α spectroscopy studies and related nuclear structure studies.

* Corresponding author.
E-mail addresses: N.Tortorelli@gsi.de, N.Tortorelli@lmu.de (N. Tortorelli).
[1] Deceased.

https://doi.org/10.1016/j.nuclphysa.2024.122967
Received 26 July 2024; Received in revised form 30 September 2024; Accepted 30 September 2024

Available online 3 October 2024

1. Introduction

Ever since the discovery of the phenomenon in 1899 by Rutherford [1], and the empirical evidence of the relationship between the half-lives and decay energies in 1911 by Geiger and Nuttall [2], nuclear alpha decay has been used in a large number of applications. The pioneering work by Rutherford studying the interaction of alpha radiation with matter led to the discovery of the atomic nucleus. The role of alpha spectroscopy as an important experimental nuclear physics technique was strengthened with the theoretical explanation of the alpha decay mechanism using quantum-mechanical tunneling by Gamov in 1928 [3]. Starting from the second half of the last century, alpha spectroscopy has been employed in various scenarios as a powerful identification method of radioactive isotopes [4], especially as a diagnostic method in radioactive ion beam facilities. High-resolution alpha spectroscopy can provide a unique fingerprint of an alpha-decaying nuclide in terms of the characteristic alpha energies and branching ratios. The identification of long alpha chains has been heavily used in the search for new super-heavy elements [5] and studies of actinides [6]. The population of direct alpha decaying nuclear isomers has been employed in characterizing the angular momentum in various nuclear reactions: fragmentation [7], fusion [8], and recently multi-nucleon transfer reactions [9]. In addition, the characterization of alpha-decaying nuclides has aided nuclear structure studies in the lead region in combination with high-resolution laser spectroscopy [10] or time-of-flight mass spectrometry [11]. This paper discusses the implementation of an alpha spectroscopy setup at the FRS Ion Catcher (FRS-IC) at GSI [12]. The FRS-IC has been designed for high-precision experiments with stopped exotic nuclei produced by projectile fragmentation and fission. The FRS Ion Catcher consists of the cryogenic gas-filled stopping cell (CSC) [13–15], an RFQ transport and diagnostics beam line (DISTRICT), and a multiple-reflection time-of-flight mass spectrometer (MR-TOF-MS) [16–18]. Alpha spectroscopy of the stopped exotic nuclei using silicon detectors has been employed as one of the key tools for physics measurements as well as a systematic characterization tool of the FRS-IC. The first studies were performed by investigating the decay chains of ^{218}Rn, ^{219}Rn, ^{221}Ac, ^{220}Fr and ^{223,224}Th produced by projectile fragmentation of ^{238}U. Another key physics result from the FRC-IC employing alpha spectroscopy was the determination of the angular momentum distribution of ^{211}Po following the fragmentation reaction ^{238}U+ ^{9}Be at relativistic energies [19]. Including the mass-selection method shown in that paper, it is possible to perform decay spectroscopy of short-lived nuclides having a parent's background-free decay, exemplified by the half-life measurement for the very short-lived isotope ^{215}Po ($t_{1/2} = 1.78$ ms) which we report here.

2. FRS Ion Catcher (FRS-IC)

The FRS-IC is located at the final focal plane of the FRagment Separator FRS at GSI [20]. It is an experimental facility where the advantages of ISOL and in-flight separator techniques are elegantly combined to enable low-energy, high-precision experiments of exotic ions produced at relativistic energies.

Ions extracted from the heavy-ion synchrotron SIS-18 impinge on a production target at the FRS to produce projectile or fission fragments. The spatial separation of the fragments is performed by two-fold magnetic rigidity analysis in front of and behind a mono-energetic degrader placed at the central focal plane. The very short flight time of a few hundred nanoseconds through the FRS gives access to very short-lived nuclides and allows isotopes to be identified using the in-flight particle detectors of the FRS on a ion-by-ion (event-by-event) basis. The in-flight separation technique is particularly challenging for nuclei produced at relativistic energies because of the large longitudinal and transverse emittance of the ions after production and slowing down. The ions are first range-bunched [21] using a dispersive magnetic stage and a mono-energetic degrader system to reduce the range spread of the ions by up to an order of magnitude, which makes stopping accordingly more efficient.

After production and separation, the ions are then slowed down and finally stopped and thermalized in a gas-filled stopping cell. Typically, the stopping cell is filled with helium gas at a pressure on the order of 100 mbar at cryogenic temperature. The thermalized ions are then guided to the exit side of the cell using static DC electric fields, focused to an exit nozzle using an RF carpet applying AC and DC fields, and extracted as an ion beam with low kinetic energy, see details in [13–15]. The ions extracted from the stopping cell may be pre-filtered for a certain mass-over-charge range of interest via an extraction RF quadrupole (RFQ) operated as quadrupole mass filter (QMF) [22]. The ions then enter a low-energy (∼eV) RFQ beamline which provides first diagnostics tools, calibration ion sources, transport, isolation as well as cooling and trapping; from here on referred to as the DISTRICT module (DISTRICT, Diagnostics, Ion Sources, Transport, Isolation, Cooling and Trapping module). The first alpha spectroscopy devices of the FRS-IC are situated in the first DISTRICT vacuum chamber. DISTRICT is equipped with a remote-controlled translation stage that accommodates two silicon detectors, a channeltron detector and an RFQ segment such that the ions can either be identified and quantified by their alpha-decay energy and half-life or transmitted downstream to the multiple-reflection time of flight mass spectrometer (MR-TOF-MS). The MR-TOF-MS itself is a powerful and universal mass spectrometer with single-ion sensitivity, a mass resolving power (FWHM) as high as 10^6 and mass accuracy of low 10^{-8} [23]. In the MR-TOF-MS, the ions are accumulated, cooled by collisions with helium buffer gas in an RF trap system, and then injected as bunches into the time-of-flight analyzer, where they fly for a certain number of turns until they exit the analyzer and impinge on a time-of-flight detector for mass measurements or a Bradbury-Nielsen gate for mass selection followed by another silicon detector. This is the second alpha spectroscopy device of the FRS-IC. To illustrate this description a sketch of this facility is shown in Fig. 1. However, an in-depth description of the experimental setup and the working principle of the full FRS-IC setup is not within the scope of this work and is described in detail elsewhere [12,15]. The following presentation of the experimental setup will focus on the alpha spectroscopy systems of the FRS-IC.

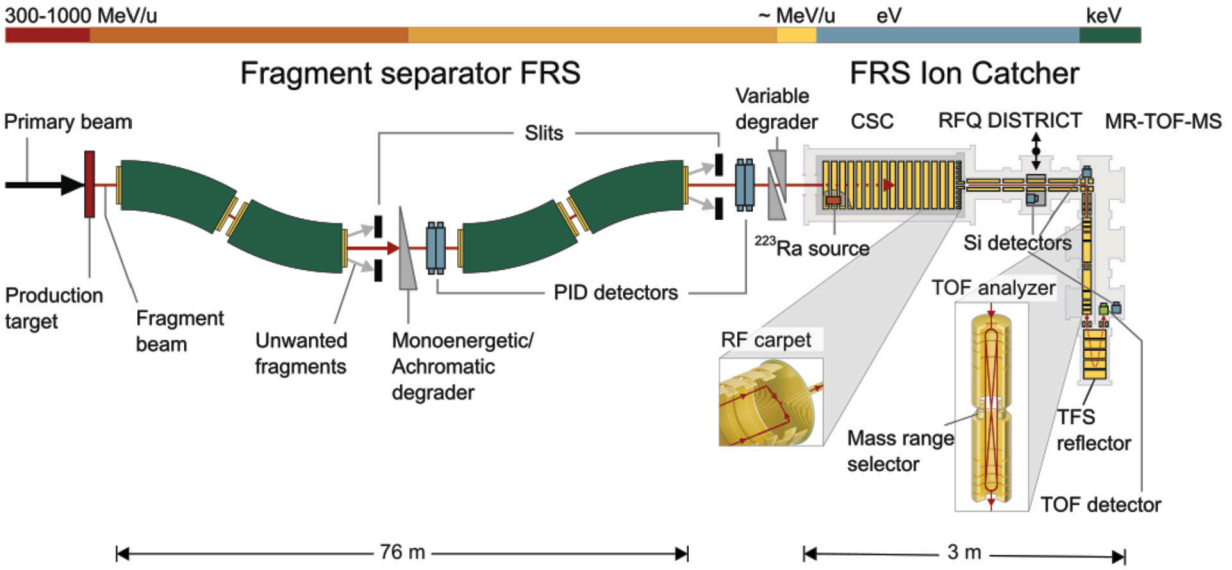

Fig. 1. Schematic layout of the fragment separator FRS together with the FRS Ion Catcher.

3. FRS-IC alpha spectroscopy systems

The alpha spectroscopy setup installed in the first DISTRICT module contains two identical detector setups on a remote-controlled translation stage. This redundancy additionally facilitates fast switching between detectors and reduced decay background by switching to a clean detector. The Si detectors used are silicon ion-implanted charged particle detectors manufactured by ORTEC from the ULTRA series with 100 µm depletion depth and 150 mm^2 active area (Ortec Ultra $BU-016-150-100$ bakeable). The detector and its data acquisition (DAQ) system (CAEN DT5780SDM) are optimized to achieve optimum energy resolution, typically sigma between 30 to 60 keV are achieved.

In order to characterize the performance and optimize the system offline, an internal source emitting alpha-decaying nuclei is needed. For this purpose, several ion sources have been installed, a ^{223}Ra alpha recoil source with a half-life of ≈ 11 days has been used initially, whereas more recently a ^{228}Th source with a half-life of ≈ 2 years was installed at the entrance side of the CSC. As alpha recoils are typically emitted with ≤ 100 keV energy, they can easily be stopped in the CSC and delivered to the DISTRICT setup. In addition a 3-line alpha source containing ^{239}Pu, ^{241}Am and ^{244}Cm is installed directly in DISTRICT at an off-axis location.

Ions from the internal sources and those from online production are transported to the setup and the energy of the alpha particles emitted can be measured. However, in order to not accumulate long-lived activity directly on the detector surface, an aluminum collection foil with thickness of 100 µg/cm^2 or 200 µg/cm^2 is installed in front of each detector. The foils are placed 5 mm in front of the detector surface, which limits the maximum solid angle covered by the Si detector. In our case the detector covers a solid angle of $d\Omega/4\pi = 0.21$, assuming a point-like implantation spot at the center of the foil. Simulations suggest an implantation spot size of less than 1 mm; thus, the point-like spot is a valid assumption.

The performance of the alpha detector permanently installed as part of DISTRICT will be reported in the following paragraph. The alpha detection system located at the end of the MR-TOF-MS will be discussed in Sec. 5.

3.1. Performance characterization

Recoiling ions from the ^{223}Ra source were extracted and collected on the foil in front of one of the Si detectors. Fig. 2 shows typical alpha energy spectra as obtained with DISTRICT under three different scenarios: no foil installed, 100 µg/cm^2 and 200 µg/cm^2 foils installed. Without a foil installed, the setup reaches an alpha energy resolution of about 14 keV in sigma, about a factor of two lower compared to the manufacturer's specifications. However, with a foil installed the energy resolution of the alpha spectroscopy detectors is dominantly limited by the collection foils themselves, as those cause additional peak broadening due to two effects. Firstly, due to direct energy straggling σ_{direct} of the alpha particles penetrating through the foil and, secondly, due to peak broadening σ_{angle} caused by alpha particles penetrating the foil under different angles given by the solid angle coverage of the detector, which results in a variation of effective thickness when penetrating the foil [24]. As shown in Fig. 2, a peak width of $\sigma_{exp} = 26$ keV and $\sigma_{exp} = 48$ keV could be achieved for 100 µg/cm^2 and 200 µg/cm^2 thick aluminum foils, respectively. The peak broadening by the foil setup was further estimated via SRIM energy loss calculations. In Table 1, the experimental resolution is compared to the estimates. The σ_{direct} and σ_{angle} values are quadratically added to the intrinsic detector resolution of 14 keV achieved without foil, which gives an estimate for the expected total peak width σ_{total} to be obtained when using collection foils. The calculated peak widths are in good agreement with the experimental results and confirm the limits set by the foils; no measurement was performed for a foil thickness of 50 µg/cm^2. It is further possible to employ even thinner foils, such as e.g. 10 µg/cm^2 as recently demonstrated in [25].

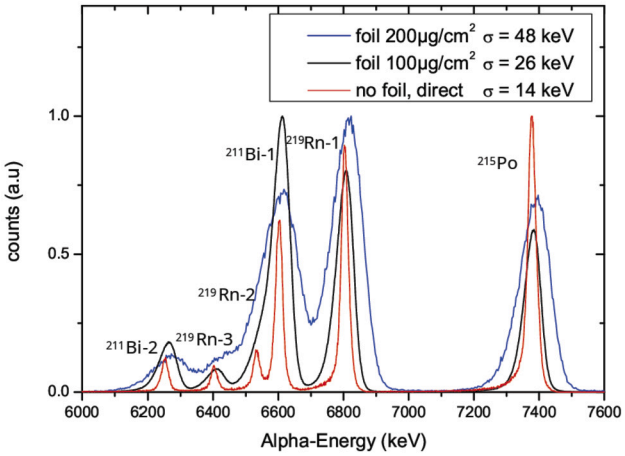

Fig. 2. Alpha decay spectrum of ^{219}Rn, originating from the internal ^{223}Ra source and measured using the silicon detector of the DISTRICT with Al collection foil thicknesses of 200 µg/cm^2 and 100 µg/cm^2, respectively, placed in front of the detector surface in comparison to the resolution achievable with the bare detector. The measurements are performed under different cleanliness and extraction conditions, which results in different elements to be extracted and transported with different efficiencies. The three datasets were not acquired during identical acquisition times and no normalization was applied, such that the number of counts is plotted in arbitrary units.

Table 1
Comparison of the peak broadening induced by aluminum foils placed in front of the silicon detector surface to prevent long-lived activity deposition on the detector. The silicon detector setup has an intrinsic alpha energy resolution of 14 keV. σ_{direct} refers to the contribution due to direct energy straggling of the alpha particles penetrating through the foil, while σ_{angle} takes into account the peak broadening contribution caused by the dependency for the alpha particles on the energy from the penetration angle into the foil. The quadratic sum of these two contributions is given as σ_{total}. σ_{exp} refers to the experimentally measured energy resolution.

Al foil µg/cm^2	σ_{direct} (keV)	σ_{angle} (keV)	σ_{total} (keV)	σ_{exp} (keV)
200	8.8	37	40.9	48
100	6.1	18	24.2	26
50	4.3	11.3	19.3	-

However, thicker foils are typically considered more stable and the reliability of the setup in DISTRICT, a standard commissioning and characterization tool, was considered to be more important. As such, foils with a thickness of 100 µg/cm^2 were chosen for standard operation and were used during all measurements reported in this paper. Under these conditions alpha spectroscopy of separated secondary beams can be performed with energy resolutions of about 60 keV sigma.

4. Optimization of the FRS-IC performance

The following section is devoted to offline and online procedures and technical developments to optimize the performance of the FRS Ion Catcher setup.

4.1. Offline optimization of the FRS-IC

To prepare the setup to transport and then study the ions of interest in a certain mass range, preparatory offline measurements are required to characterize and optimize individual subsystems. The FRS-IC facility consists of multiple filtering and analysis stages composed of detectors and mass filters [22]. Offline characterization of the ion extraction and detection performance from the gas cell is enabled by the internal alpha recoil ion source installed in the entrance region (attached to the first electrode ring) of the DC electrode system of the CSC. Ions traversing the CSC on off-axis trajectories are guided to the extraction nozzle at the exit side by the RF carpet. The RF carpet provides a DC gradient towards its axial center and a repelling RF potential. Thus, it guides ions towards the exit nozzle, where they are dragged via a supersonic gas jet out of the CSC into a subsequent RFQ, acting as an ion guide and mass filter, with a mass resolving power of 10 (using FWHM), while achieving a transmission efficiency of about 80% [26].

The mass filter allows us to select the mass region of interest or a certain charge state and to break apart the molecular ions during the transport. Depending on the setting of the RFQ as an ion guide or mass filter, the extracted ions arrive at DISTRICT either

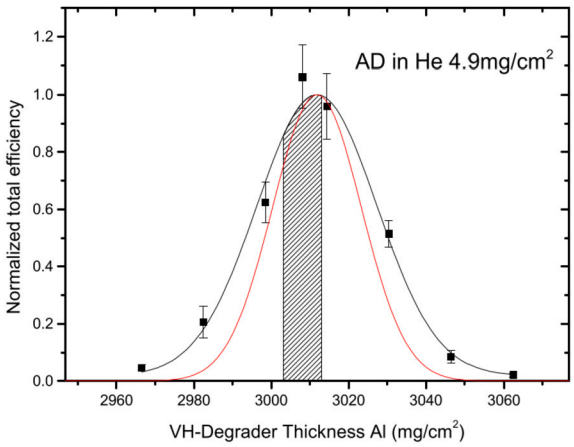

Fig. 3. Stopping range distribution of ^{223}Th ions in the cryogenic stopping cell determined as a function of the variable degrader thickness. The black solid curve shows a Gaussian fit to the experimental normalized total efficiency. The expected range distribution of a monoenergetic beam in red is shown with straggling in the variable degrader. The hatched region indicates the areal density (AD) covered by the stopping cell and it is arbitrary placed in this plot to indicate the CSC thickness in relation to the momentum spread of the incoming beam. (For interpretation of the colors in the figure(s), the reader is referred to the web version of this article.)

in a wide or narrow mass range. Here, alpha spectroscopy can be performed using the silicon detectors previously introduced. The alpha spectroscopy is of primary importance, as it enables system optimization through the utilization of radioactive atomic species due to the precise knowledge we possess regarding the generating sources and intrinsic properties of radioactive species. Using this detector, a scan of the mass-over-charge range of a certain species extracted from the CSC can be done. This allows the identification and quantification of the charge-state distribution and as such helps to prepare optimum mass-over-charge settings for the downstream beam line. Furthermore, in the case when there is no alpha emitter in the mass region of interest for the measurement, the identification of masses is done at the MR-TOF-MS once the calibration to the mass filter and the extraction is done with the internal alpha recoil ion source.

4.2. FRS-IC as alpha tagging setup

In case the ion of interest stems from a secondary beam with charge Z and mass A being far away from the primary beam, the in-flight identification based on measuring A/Q vs Z may become difficult. A non-negligible difference between calibration and operational settings may emerge due to the large difference in energy loss between the primary beam and secondary fragments, rendering the possibility of a wrong assignment of Z. In such a scenario, the FRS-IC can correct the calibration by identifying a single nuclide closer in Z to the ion of interest. This can be done either via "γ-tagging" ([27], [28]), via "mass tagging" using precision mass spectrometry with the MR-TOF-MS [29] or as "alpha tagging" using alpha spectroscopy. At the FRS-IC two separate setups have been used for alpha tagging, a single DSSD detector placed in front of the CSC and the silicon detectors within DISTRICT.

In later method, the ions are thermalized in the stopping cell and measured using a Si detector in DISTRICT. Based on available alpha decay energies the stopped ions can be identified and the in-flight identification can be updated. The method was used during multiple online experiments and demonstrates the feasibility of using the FRS-IC as a tagger for alpha decaying nuclides with half-lives from few milliseconds extended to few minutes.

4.3. Online optimization of the FRS-IC

After completing the isotope identification at the FRS, the following steps have to be taken to maximize the amount of the beam stopped in the CSC so that the maximum beam can then be transported to downstream setups for example to the MR-TOF-MS. The approach involves optimizing the homogeneous degrader of variable thickness (variable degrader) installed just before the CSC, see Fig. 1. By adjusting the thickness of the degrader, it is possible to center the mean range of the beam in the middle of the stopping cell. The ideal thickness depends on the characteristics of the species to be stopped (mainly energy and atomic number Z) and on the density of the helium gas filling the CSC. Depending on the specific experiment, the CSC is filled with helium gas with an areal density from 2 to 9 mg/cm^2. Ions were injected into the CSC, extracted and subsequently sent to DISTRICT, where they were collected on the Si detector setup. Here, they were spectroscopically identified via their characteristic alpha decay energies. To obtain the number of extracted ions of the nuclide of interest, the number of registered decay events, taking the solid angle of the detector into account, were compared to the number of isotopes identified In-Flight via the FRS detectors.

This optimization procedure allows to set the degrader to a thickness that maximizes the number of ions stopped in the CSC. Fig. 3 illustrates such a stopping range distribution (normalized) of ^{223}Th ions versus the areal thickness of the variable degrader at a CSC areal density of 4.9 mg/cm^2. The black curve represents a Gaussian fit to the experimental data points; the red curve shows a distribution expected for a monoenergetic beam, while the hatched region indicates the areal density covered by the stopping cell.

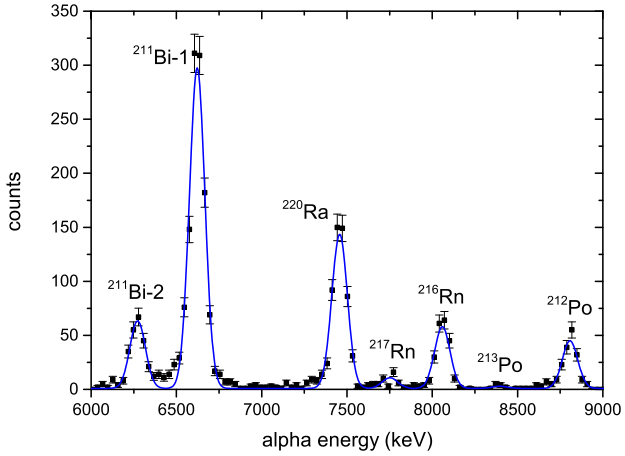

Fig. 4. Alpha-energy spectra of ^{221,220}Ra produced by ^{238}U projectile fragmentation at 1000 MeV/u at the FRS Ion Catcher, measured with the Si detector in the DISTRICT.

Once the optimal settings for stopping in the CSC have been determined, it is possible to scale the degrader thickness to stop arbitrary ions of interest, which indeed might have a different energy and Z.

5. Results

In the following section several offline and online experiments will be discussed based on data acquired using the alpha spectroscopy setups.

5.1. Alpha spectroscopy of ^{238}U projectile fragments

The alpha tagging method explained in 4.2 has been applied during a study of short-lived nuclides produced by ^{238}U projectile fragmentation at 1000 MeV/u. Combining the separation of the FRS and the selective stopping in the CSC, the decay chains of several decay chains could be measured with the Si detectors in DISTRICT. In Fig. 4, the alpha decay lines of ^{221}Ra and ^{220}Ra and their daughters are shown.

The silicon detectors were initially calibrated using the ^{223}Rn decay chain from the internal source inside the CSC and alpha lines from the 3-line alpha source installed at DISTRICT. This showed that, a linear calibration function with only a small quadratic correction, contributing to systematic shift of about < 2 keV, could be used. In order to determine the alpha energies of the projectile fragments all peaks were fitted with Gaussian and exponentially modified Gaussian (HyperEMG) line shapes [30]. As during the online data collection decays of long-lived ^{211}Bi, previously collected on the foil, were also recorded, those were used to re-calibrate and adjust for gain drifts of the pre-amplifiers through out the experiment. To the uncertainty obtained via the fitting and calibration procedure a systematic uncertainty of 5 keV was added accounting for the difference in energy loss in the aluminum foil between different isotopes and alpha energies. The uncertainty due to the recoil distribution of the alpha decaying daughters has not been added since the energy difference was negligible. The new measured Q-alpha values are listed in Table 2.

Fig. 5 shows the deviation between the measured Q-alpha values from ^{238}U projectile fragments and previous literature. The measured Q-alpha values reproduce known literature values well. The deviation is characterized by a normal distribution, with a Birge ratio of 0.5, and as a consequence no further additional systematic uncertainties were considered.

Noteworthy is the measurement of ^{221}Ac, whose Q_α measurement was done in the past as part of the decay chain of ^{225} Pa [6]. There, two close-lying, about 50 keV apart, peaks were identified in the energy spectrum and due to the limited pre-separation capabilities (using a He-jet technique without mass resolution and mass identification) it could not be ruled out which peak should belong to the ^{221}Ac ground state or might belong to different species. Moreover, also the evaluator of NNDC [31] puts the existence of this second alpha line as belonging to the decay of ^{225} Pa in doubt. However, already in [32], and more recently in [33], suiting mass separated samples, the gs-gs alpha decay was reported with a good precision and the existence of the spurious peak, as belonging to the decay of ^{225} Pa, was refuted. In the work presented here, the direct In-Flight production and separation combined with the selective stopping in the CSC has been applied and this strongly suppresses neighboring isotopes [34]. In our case there is no identification of a secondary peak in our spectrum. Further, we were able to rule out possible long-lived contamination via a time-resolved alpha measurement, see Sec. 5.2. Our Q_α energy of 7778(10) keV is in good agreement with the Q_α energy reported in [32] and [33] providing a confirmation of the reliability of the FRSIC data.

The Q_α values for the isotopic chains of Th, Ac, Ra, Fr, Rn, At and Po are shown in Fig. 6 as a function of the neutron number N using open symbols. Values of isotopes determined in this work are shown as solid symbols. The well known characteristic maximum of the Q_α values around $N = 128$ can be seen. The known crossings of the Q_α values of the astatine and radon chains at $N = 131$ and radium chains at $N = 133$ are reproduced in our measurements, where the open symbol (literature values) are overlapped by the

Table 2
Alpha decay energies (E_α) and Q-alpha values (Q_α) of radioactive nuclei measured using the FRS Ion Catcher produced online via ^{238}U projectile fragmentation at 1000 MeV/u. 'Level^{lit}' refers to alpha transitions into excited states, energy values were taken from literature [31].

Isotope ^{A}X	Level^{lit} (keV)	E_α (keV)	Q_α (keV)
^{211}Po	0	7450 (7)	7595 (7)
^{211m}Po-1	1633	7273(5)	9047 (5)
^{211m}Po-2	0	8877 (13)	
^{211m}Po-3	897.8	78000 (28)	
^{212}Po	0	8801 (13)	8970 (13)
^{213}Po	0	8387 (46)	8548 (47)
^{214}Po	0	7706 (37)	7853 (38)
^{216}At	0	7792 (16)	7941 (16)
^{215}Rn	0	8692 (19)	8849 (19)
^{216}Rn	0	8055 (15)	8207 (15)
^{217}Rn	0	7750 (26)	7896 (26)
^{218}Rn	0	7143 (26)	7277 (26)
^{217}Fr	0	8313 (10)	8469 (10)
^{219}Ra-1	0	7990 (15)	8135 (11)
^{219}Ra-2	315.8	7674 (13)	
^{220}Ra	0	7457 (9)	7595 (9)
^{221}Ac-1	0	7640 (11)	7778 (10)
^{221}Ac-2	209	7432 (13)	
^{223}Th	140.0	7297 (11)	7571 (11)
^{224}Th-1	0	7164 (13)	7296 (12)
^{224}Th-2	178.4	6996 (20)	

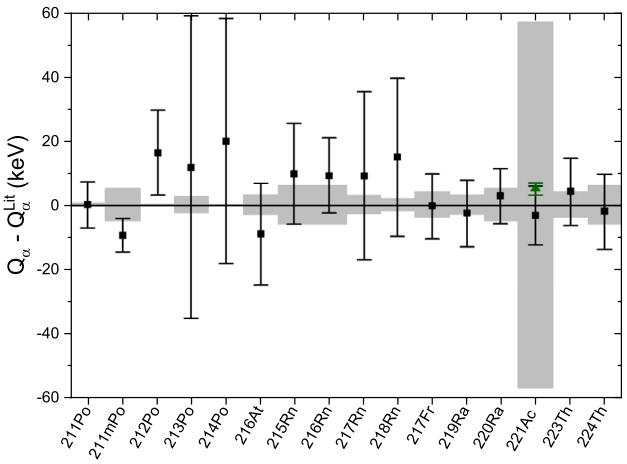

Fig. 5. Q_α values of ^{238}U fragmentation products measured at the FRS Ion Catcher in comparison to their literature values, taken from [31]. An updated value for ^{221}Ac was recently reported in [33], indicated by the green data point.

solid symbol (measured values). A detailed discussion is beyond the scope of this paper, but it demonstrates the potential of FRS-IC alpha spectroscopy system for nuclear structure studies of actinides.

5.2. *Half-life measurement of ^{221}Ac and ^{223}Th*

Combined alpha and half-life measurements of ^{221}Ac and ^{223}Th were preformed. To do so, the DISTRICT data acquisition system was set to record energy and time of each event, whereas the start signal for the clock was given by a trigger signal from the FRS data acquisitions. The spill length / bunch length of the ^{238}U primary beam was set to less then 10 ms. Under those conditions, only the extraction time from the CSC to the silicon detector setup causes additional delays and limits the technique to nuclei with half-lives of above a few tens of ms. In the analysis one can then gate on a specific alpha energy range and evaluate the temporal evolution of those decays.

In Fig. 7, the results of the time-resolved decays curves of ^{223}Th and ^{221}Ac are plotted after gating on their characteristic dominant alpha decay branch. The observed pattern can be well described by a Gaussian peak convoluted with an exponential decay function.

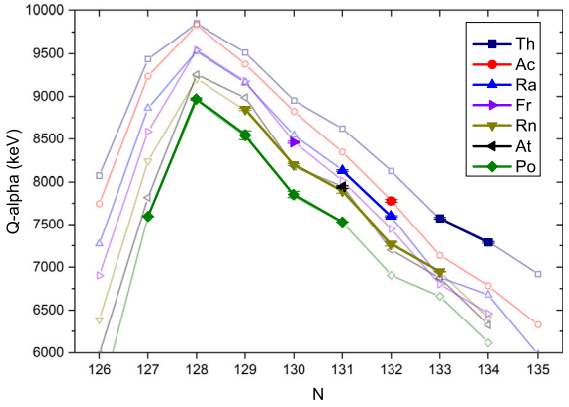

Fig. 6. The Q_α values of the decay of the radio-isotopes measured at the FRS Ion Catcher after their production via projectile fragmentation of ^{238}U at 1 GeV/u are plotted as a function of the neutron number N. The Q_α values are represented as solid symbols. The literature values are the open symbols.

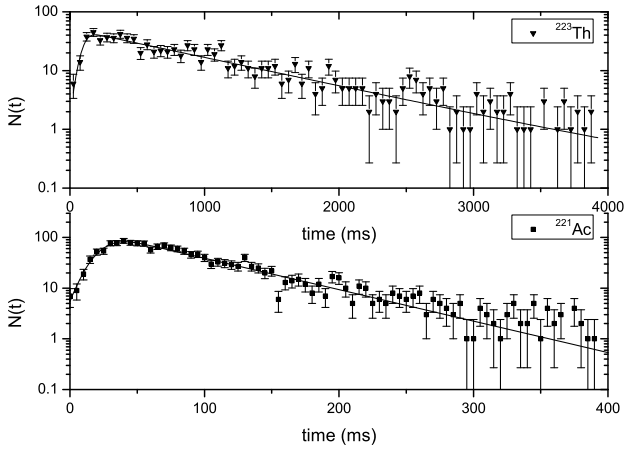

Fig. 7. Half-life measurement of ^{223}Th and ^{221}Ac. The number of ^{223}Th (^{221}Ac) decay events is plotted as a function of the time elapsed after the injection of the ions into the CSC. The fit function consists of a Gaussian plus an exponential decay function used to determine the half-life.

It considers the initial activity increase dominated by the ion extraction from the CSC and the exponential decay dominating after all ions have been extracted and collected on the foil in front of the silicon detector. The solid line represents the fit to the data.

The half-lives of ^{223}Th and ^{221}Ac can then be determined in two ways: (i) by gating directly on the alpha decay line of the isotope as shown in Fig. 7 or (ii) by gating on the alpha decay energies of much shorter lived direct daughter isotopes. The method of filtering on the nuclide daughters originates from the need to validate the half-live and identification of ^{221}Ac.

For ^{223}Th, it was possible to determine its half-life by filtering on the alpha decay of ^{223}Th and, in addition, filtering the alpha decay of its daughter nuclides ^{219}Ra and ^{215}Rn. Since the daughter nuclides ^{219}Ra and ^{215}Rn have a very short half-life compared to that of ^{223}Th the evolution of their decays is dominated by the slower decay rate of ^{223}Th. Similarly, for ^{221}Ac, it was possible to derive its half-life by filtering the alpha decay of the daughter nuclides ^{217}Fr and ^{213}At. As for the case above, these daughter nuclides have significantly shorter half-lives than ^{221}Ac. This indirect method agrees well with direct determination of the half-life of ^{221}Ac. In the case of ^{221}Ac an abundance of events beyond 300 – 400 ms is not well described by the fit and may have suggested the presence of a long-lived contaminant. However, a similar long-lived component did not appear in the decay patterns of ^{217}Fr and ^{213}At and as such could be ruled out.

The half-lives of ^{223}Th and ^{221}Ac determined here, are listed in Table 3. The half-lives of ^{221}Ac is in good agreement with the known literature values from the ENSDF [31] compilation and with a recent result of [33]. Our result for ^{229}Th further reinforce a half-life of around 600 ms as suggested by [35] and [36], which had been in conflict with a half-life of 900(10) ms as obtained by [37].

5.3. Angular momentum distribution of ^{211}Po

Measuring the fraction of the nuclei produced in their ground state and isomeric states can provide helpful information about the angular momentum distribution populated during the fragmentation process. At the FRC-IC, ^{211}Po was chosen as a suitable candidate to be studied in this context. ^{211}Po has a rich level scheme, including multiple high-spin isomeric states. Its first isomeric state with

Table 3
Half-lives of ^{223}Th and ^{221}Ac determined by time-resolved alpha spectroscopy. The literature reference values are taken from ENSDF [31].

Isotope ^{A}X	$t^{lit}_{1/2}$ (ms)	Ref.	$t_{1/2}$ (ms)
^{223}Th	600 (20)	[35]	618 (47)
	660 (10)	[36]	
	900 (10)	[37]	
^{221}Ac	52 (2)	[6]	49.5 (30)

Table 4
In this table the isomer ratio R_{exp} of ^{211}Po compared to analytical calculations [42] R^{f} and predictions from the ABRABLA code [44] $R^{ABRABLA}$ are listed, using the sharp cut-off (R_{th}) and the spin-mixing approach (R_{th-mix}). The measurements for spin states $25/2^+$ and $9/2^+$ have been performed after the higher-lying states have decayed by internal conversion, so the sum of the isomeric ration for $25/2^+$ and $9/2^+$ ends up to 100%. The gamma spectroscopy measurements, as for the high spin state $43/2^+$, are treated independently and the 8% from the $43/2^+$ state does not need to be combined with the isomeric ratios of the $25/2^+$ and $9/2^+$ states.

	R_{exp}	R^{f}_{th}	$R^{ABR.}_{th}$	R^{f}_{mix}	$R^{ABR.}_{mix}$	Ref
$9/2^+$	0.26(5)	0.86	0.71	0.81	0.65	
	0.29(9)	–	–	–	–	[19]
$25/2^+$	0.74(10)	0.11	0.28	0.19	0.35	
	0.71(23)	–	–	–	–	[19]
$31/2^-$	–	0.05	0.12	0.08	0.20	
$43/2^+$	0.08(1)	–	–	–	–	[41]
	–	0.004	0.03	0.006	0.05	

a spin of ($\frac{25}{2}^+$) and half-life of 25.2 s corresponds to an excitation energy of 1462 keV. The ^{211}Po ground state has a spin of ($\frac{9}{2}^+$) and a half-life of 516 ms. Both states decay via alpha emission. Its properties have in the past been exploited to estimate angular moment transfer in various direct reactions [38–40] including recent work studying incomplete fusion [8] and multi-nucleon transfer reactions [9]. It makes ^{211}Po an ideal candidate to study angular momentum distribution created in in-flight projectile fragmentation by measuring the isomeric ratio (R), i.e. the ratio of isomeric over ground-state population cross section, via alpha spectroscopy, complementing previous work done via gamma spectroscopy [41] and high resolution mass spectrometry [19].

At the FRS Ion Catcher, the production of the ($\frac{25}{2}^+$) isomeric and ($\frac{9}{2}^+$) ground state in ^{211}Po were measured via alpha spectroscopy, while higher-lying isomeric states can be studied by γ spectroscopy. Here, the alpha-decay data was combined with isomeric ratio measurements performed by the RISING collaboration using the same primary beam and target conditions [41]. In our case, an isomeric ratio of 0.74(10) was measured in agreement with our previous result of 0.71(23) obtained via mass spectrometry [19], but about a factor of 2 more precise.

In order to link the isomeric ratio to the angular momentum distribution during production we consider two estimates of the distribution, an analytic approach [42] and one based on macroscopic geometric calculations obtained via ABRABLA [43], [44]. From each distribution, the isomeric ratio can then be calculated via either a sharp cut-off model [42] and a model introducing some limited mixing [8]. The sharp cut-off model assumes that all potential states above a certain isomeric state will populate this particular state. The probability populating this state can then be obtained by integrating over the angular momentum distribution above. Following the assumption of Gasques [8], an empirical spin-state mixing can be introduced, where the cut-off (so-called J_{eff} cut-off) takes into account the neutron evaporation and the cascade of gamma rays from the initial compound nucleus to the final state in a way that the J_{eff} cut-off corresponds to the angular momentum where the isomeric state reaches its maximum at the spin of the excited state, see details in Gasques [8].

The resulting isomer ratios are listed in Table 4, where a comparison is presented between experimental results and theoretical isomeric ratios for the four sets of theoretical calculations. Our results are in agreement with previous experimental isomeric ratio measurements [45,41]. However, the theoretical predictions overestimate the experimental isomer ratios ones by about a factor of 3 to 10 and consistently predict a much stronger population of the $9/2^+$ ground state compared to the first excited $25/2^+$ isomeric state. This further highlights that the angular momentum distribution arising from fragmentation is still not fully understood, and new input from isomer ratio measurements is needed to provide insight into the mechanism of populating isomeric states.

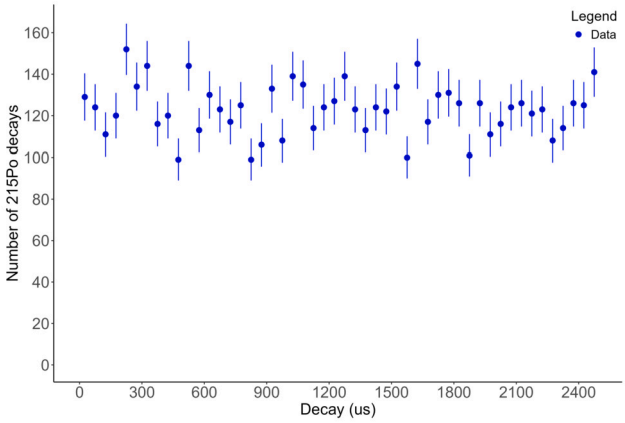

Fig. 8. α-decay measurement of ^{215}Po isotopes without gating on the ^{215}Po mass. The decay of ^{215}Po ions is masked by the population from ^{219}Rn.

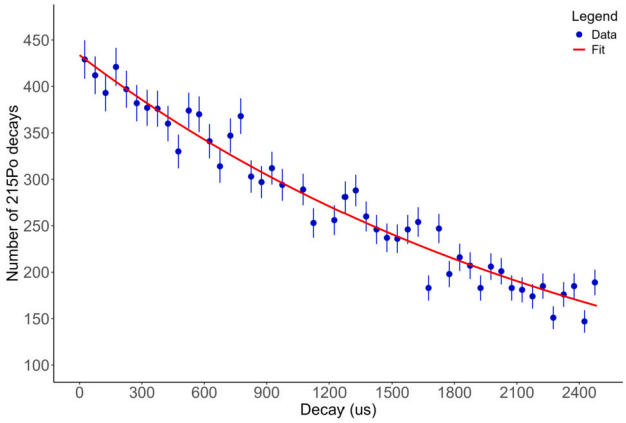

Fig. 9. α-Decay measurement of ^{215}Po with the gate set on its time-of-flight mass spectrum.

5.4. Mass selective decay spectroscopy

An additional important method applied to the α-decay spectroscopy done at the FRS-IC is the α-decay spectroscopy with prior high-resolution mass-selection. This method has already been used for a proof-of-concept of isomer separation [19]. The method exploits a Bradbury–Nielsen Gate (BNG) installed at the detector plane of the MR-TOF-MS followed by a Si detector. The BNG is a thin grid that, if pulsed, deflects unwanted ions and lets the ion of interest pass through. In our case the mass spectra were background free due to a suppression of at least 4 order of magnitude for the parents nuclei when using the BNG selection.

In this work, mass-selective decay spectroscopy has been performed with short-lived ^{215}Po produced via decay from the ^{223}Ra source. In order to efficient transport and identify ^{215}Po, with a half-life of only 1.781(3) ms [31], the MR-TOF was operated at 400 Hz, corresponding to a cycle time of 2.5 ms. Ions were transported through the setup, bunched via the injection trap at the MR-TOF, transported to the silicon detector behind the BNG. The time distribution of the ^{215}Po alpha decays was measured relative to the ion ejection from the injection trap. Plotting the number of ^{215}Po ions versus time, without any mass selection, no half-life can be measured; see Fig. 8. In this case, the decay of ^{215}Po ions is masked by the population from the parent isotope ^{219}Rn with a half-life of 3.96 s, which is also generated from the ^{223}Ra source. When the Bradbury-Nielsen gate after the time-of-flight analyzer is set to remove other species and only to transport ^{215}Po ions to the silicon detector, a decay curve for the same plot can be seen (Fig. 9).

Two series of data for the mass selective setting have been recorded: a high statistics file containing $\sim$ 13000 decays and a low statistics file containing $\sim$ 1000 polonium decays. Both data sets have been evaluated, and a weighted mean has been calculated. The results are summarized in Table 5.

Our new result of 1.774(55) ms is in good agreement with previous literature and shows the potential for future mass-separated decay spectroscopy of ground and isomeric states.

Table 5
Half-life measurement of ^{215}Po ions. Two independent measurements have been evaluated and a weighted mean has been calculated. The number of decays N recorded and resulting half-life $t_{1/2}$ are reported.

Measurement	N	$t_{1/2}$ (μs)
I	12864	1732(56)
II	934	1969(263)
weighted mean		1774(55)

6. Summary

In this work, the FRS Ion Catcher facility has been described with special emphasis on its capabilities for alpha-decay spectroscopy. Procedures for off- and online setup optimization were presented, and some prototypical results were reported. Experimental campaigns at the FRS-IC have led to a broad scope of investigated phenomena that could be studied by alpha spectroscopy. The device is able to identify secondary fragments with half-lives down to about 2 ms, measuring their mass, the alpha-decay energy and the decay time. Another important aspect is the ability of the FRC-IC to combine alpha spectroscopy and mass spectrometry of thermalized exotic nuclei. This allows for an investigation of the angular momentum distribution generated by the projectile fragmentation process. Together to this, this paper proves the FRS-IC to be able to unveil the nuclear structure of exotic nuclei as showed in Sec. 5.3, Sec. 5.1 and Sec. 5.3.

CRediT authorship contribution statement

Nazarena Tortorelli: Writing – review & editing, Writing – original draft, Supervision, Data curation. **Moritz Pascal Reiter:** Writing – review & editing, Methodology, Investigation, Formal analysis, Data curation. **Ann Kathrin Rink:** Formal analysis, Data curation. **Sivaji Purushothaman:** Resources, Methodology, Conceptualization. **Samuel Ayet San Andrés:** Writing – review & editing, Investigation. **Julian Bergmann:** Software. **Timo Dickel:** Writing – review & editing, Supervision, Methodology, Funding acquisition, Data curation, Conceptualization. **Marcel Diwisch:** Investigation. **Jens Ebert:** Investigation. **Florian Greiner:** Investigation. **Emma Haettner:** Investigation. **Christine Hornung:** Investigation. **Aleksandra Kelic-Heil:** Investigation. **Ronja Knoebel:** Investigation. **Wayne Lippert:** Investigation. **Ivan Miskun:** Investigation. **Iain D. Moore:** Investigation. **Stephane Pietri:** Investigation. **Wolfgang R. Plaß:** Writing – review & editing, Investigation. **Ilkka Pohjalainen:** Investigation. **Andrej Prochazka:** Investigation. **Christoph Scheidenberger:** Investigation. **Maya Takechi:** Investigation. **Peter G. Thirolf:** Writing – review & editing, Supervision. **Helmut Weick:** Investigation. **Xiaodong Xu:** Investigation.

Declaration of competing interest

The authors declare the following financial interests/personal relationships which may be considered as potential competing interests: Nazarena Tortorelli reports financial support was provided by GSI Helmholtzzentrum für Schwerionenforschung. If there are other authors, they declare that they have no known competing financial interests or personal relationships that could have appeared to influence the work reported in this paper.

Data availability

Data will be made available on request.

Acknowledgement

This work was supported by GSI R&D LMTHI 2023, by the German Federal Ministry for Education and Research (BMBF) under contracts no. 05P12RGFN8, 05P16RGFN1 and 05P21RGFN1, by Justus-Liebig-Universität Gießen and GSI under the JLU-GSI strategic Helmholtz partnership agreement, by HGS-HIRe and by the Hessian Ministry for Science and Art (HMWK) through the LOEWE Center HICforFAIR.

References

[1] E. Rutherford, Uranium radiation and the electrical conduction produced by it, Philos. Mag. 47 (1899) 109, http://cds.cern.ch/record/261896.
[2] H. Geiger, J. Nuttall, The ranges of the α particles from various radioactive substances and a relation between range and period of transformation, Lond. Edinb. Dublin Philos. Mag. J. Sci. 22 (130) (1911) 613–621, https://doi.org/10.1080/14786441008637156.
[3] G. Gamow, Zur quantentheorie des atomkernes, Z. Phys. 51 (3–4) (1928) 204–212, https://doi.org/10.1007/BF01343196.
[4] K. Siegbahn, P. Axel, Alpha-, beta-, and gamma-ray spectroscopy, Am. J. Phys. 34 (3) (1966) 275–276, https://doi.org/10.1119/1.1972911.
[5] P.J. Karol, R.C. Barber, B.M. Sherrill, E. Vardaci, T. Yamazaki, Discovery of the element with atomic number Z = 118 completing the 7th row of the periodic table (iupac technical report), Pure Appl. Chem. 88 (1–2) (2016) 155–160, https://doi.org/10.1515/pac-2015-0501.

[6] J. Borggreen, K. Valli, E.K. Hyde, Production and decay properties of protactinium isotopes of mass 222 to 225 formed in heavy-ion reactions, Phys. Rev. C 2 (1970) 1841–1862, https://doi.org/10.1103/PhysRevC.2.1841.

[7] S. Pal, R. Palit, Angular momentum population in fragmentation reactions, Phys. Lett. B 665 (4) (2008) 164–167, https://doi.org/10.1016/j.physletb.2008.06.040.

[8] L.R. Gasques, M. Dasgupta, D.J. Hinde, T. Peatey, A. Diaz-Torres, J.O. Newton, Isomer ratio measurements as a probe of the dynamics of breakup and incomplete fusion, Phys. Rev. C 74 (2006) 064615, https://doi.org/10.1103/PhysRevC.74.064615.

[9] D. Kumar, T. Dickel, A. Zadvornaya, O. Beliuskina, A. Kankainen, P. Constantin, S. Purushothaman, A. Spataru, M. Stryjczyk, L. Al Ayoubi, M. Brunet, L. Canete, C. Delafosse, R. de Groote, A. de Roubin, T. Eronen, Z. Ge, W. Gins, C. Hornung, M. Hukkanen, A. Illana, A. Jokinen, D. Kahl, B. Kindler, B. Lommel, I. Mardor, I. Moore, D. Nesterenko, D. Nichita, S. Nikas, A. Ortiz-Cortes, H. Penttilä, Z. Podolyák, I. Pohjalainen, A. Raggio, M. Reponen, S. Rinta-Antila, J. Romero, J. Saren, M. Vilen, V. Virtanen, A. Weaver, J. Winfield, First investigation on the isomeric ratio in multinucleon transfer reactions: entrance channel effects on the spin distribution, Phys. Lett. B 853 (2024) 138654, https://doi.org/10.1016/j.physletb.2024.138654.

[10] R. Ferrer, A. Barzakh, B. Bastin, R. Beerwerth, M. Block, P. Creemers, H. Grawe, R. de Groote, P. Delahaye, X. Fléchard, S. Franchoo, S. Fritzsche, L. Gaffney, L. Ghys, W. Gins, C. Granados, R. Heinke, L. Hijazi, M. Huyse, A. Zadvornaya, Towards high-resolution laser ionization spectroscopy of the heaviest elements in supersonic gas jet expansion, Nat. Commun. 8 (2017), https://doi.org/10.1038/ncomms14520.

[11] M. Rosenbusch, Y. Ito, P. Schury, M. Wada, D. Kaji, K. Morimoto, H. Haba, S. Kimura, H. Koura, M. MacCormick, H. Miyatake, J.Y. Moon, K. Morita, I. Murray, T. Niwase, A. Ozawa, M. Reponen, A. Takamine, T. Tanaka, H. Wollnik, New mass anchor points for neutron-deficient heavy nuclei from direct mass measurements of radium and actinium isotopes, Phys. Rev. C 97 (2018) 064306, https://doi.org/10.1103/PhysRevC.97.064306.

[12] W. Plaß, T. Dickel, S. Purushothaman, P. Dendooven, H. Geissel, J. Ebert, E. Haettner, C. Jesch, M. Ranjan, M. Reiter, H. Weick, F. Amjad, S. Ayet, M. Diwisch, A. Estrade, F. Farinon, F. Greiner, N. Kalantar-Nayestanaki, R. Knöbel, J. Kurcewicz, J. Lang, I. Moore, I. Mukha, C. Nociforo, M. Petrick, M. Pfützner, S. Pietri, A. Prochazka, A.-K. Rink, S. Rinta-Antila, D. Schäfer, C. Scheidenberger, M. Takechi, Y. Tanaka, J. Winfield, M. Yavor, The FRS Ion Catcher – a facility for high-precision experiments with stopped projectile and fission fragments, in: XVIth International Conference on ElectroMagnetic Isotope Separators and Techniques Related to Their Applications, December 2–7, 2012 at Matsue, Japan, Nucl. Instrum. Methods Phys. Res., Sect. B, Beam Interact. Mater. Atoms 317 (2013) 457–462, https://doi.org/10.1016/j.nimb.2013.07.063.

[13] M. Ranjan, S. Purushothaman, T. Dickel, H. Geissel, W.R. Plass, D. Schäfer, C. Scheidenberger, J. Van de Walle, H. Weick, P. Dendooven, New stopping cell capabilities: RF carpet performance at high gas density and cryogenic operation, Europhys. Lett. 96 (5) (2011) 52001, https://doi.org/10.1209/0295-5075/96/52001.

[14] M. Ranjan, P. Dendooven, S. Purushothaman, T. Dickel, M. Reiter, S. Ayet, E. Haettner, I. Moore, N. Kalantar-Nayestanaki, H. Geissel, W. Plaß, D. Schäfer, C. Scheidenberger, F. Schreuder, H. Timersma, J. Van de Walle, H. Weick, Design, construction and cooling system performance of a prototype cryogenic stopping cell for the Super-FRS at FAIR, Nucl. Instrum. Methods Phys. Res., Sect. A, Accel. Spectrom. Detect. Assoc. Equip. 770 (2015) 87–97, https://doi.org/10.1016/j.nima.2014.09.075.

[15] S. Purushothaman, M. Reiter, E. Haettner, P. Dendooven, T. Dickel, H. Geissel, J. Ebert, C. Jesch, W. Plaß, M. Ranjan, H. Weick, F. Amjad, S. San Andres, M. Diwisch, A. Estrade, F. Farinon, F. Greiner, N. Kalantar-Nayestanaki, R. Knöbel, M. Yavor, First experimental results of a cryogenic stopping cell with short-lived, heavy uranium fragments produced at 1000 MeV/u, Europhys. Lett. 104 (2013), https://doi.org/10.1209/0295-5075/104/42001.

[16] W.R. Plaß, T. Dickel, U. Czok, H. Geissel, M. Petrick, K. Reinheimer, C. Scheidenberger, M.I. Yavor, Isobar separation by time-of-flight mass spectrometry for low-energy radioactive ion beam facilities, in: Proceedings of the XVth International Conference on Electromagnetic Isotope Separators and Techniques Related to Their Applications, Nucl. Instrum. Methods Phys. Res., Sect. B, Beam Interact. Mater. Atoms 266 (19) (2008) 4560–4564, https://doi.org/10.1016/j.nimb.2008.05.079.

[17] M.I. Yavor, W.R. Plaß, T. Dickel, H. Geissel, C. Scheidenberger, Ion-optical design of a high-performance multiple-reflection time-of-flight mass spectrometer and isobar separator, Int. J. Mass Spectrom. 381–382 (2015) 1–9, https://doi.org/10.1016/j.ijms.2015.01.002.

[18] T. Dickel, W. Plaß, A. Becker, U. Czok, H. Geissel, E. Haettner, C. Jesch, W. Kinsel, M. Petrick, C. Scheidenberger, A. Simon, M. Yavor, A high-performance multiple-reflection time-of-flight mass spectrometer and isobar separator for the research with exotic nuclei, Nucl. Instrum. Methods Phys. Res., Sect. A, Accel. Spectrom. Detect. Assoc. Equip. 777 (2015) 172–188, https://doi.org/10.1016/j.nima.2014.12.094.

[19] T. Dickel, W. Plaß, S. Ayet San Andres, J. Ebert, H. Geissel, E. Haettner, C. Hornung, I. Miskun, S. Pietri, S. Purushothaman, M. Reiter, A.-K. Rink, C. Scheidenberger, H. Weick, P. Dendooven, M. Diwisch, F. Greiner, F. Heiße, R. Knöbel, W. Lippert, I. Moore, I. Pohjalainen, A. Prochazka, M. Ranjan, M. Takechi, J. Winfield, X. Xu, First spatial separation of a heavy ion isomeric beam with a multiple-reflection time-of-flight mass spectrometer, Phys. Lett. B 744 (2015) 137–141, https://doi.org/10.1016/j.physletb.2015.03.047.

[20] H. Geissel, P. Armbruster, K. Behr, A. Brünle, K. Burkard, M. Chen, H. Folger, B. Franczak, H. Keller, O. Klepper, B. Langenbeck, F. Nickel, E. Pfeng, M. Pfützner, E. Roeckl, K. Rykaczewski, I. Schall, D. Schardt, C. Scheidenberger, K.-H. Schmidt, A. Schröter, T. Schwab, K. Sümmerer, M. Weber, G. Münzenberg, T. Brohm, H.-G. Clerc, M. Fauerbach, J.-J. Gaimard, A. Grewe, E. Hanelt, B. Knödler, M. Steiner, B. Voss, J. Weckenmann, C. Ziegler, A. Magel, H. Wollnik, J. Dufour, Y. Fujita, D. Vieira, B. Sherrill, The gsi projectile fragment separator (frs): a versatile magnetic system for relativistic heavy ions, Nucl. Instrum. Methods Phys. Res., Sect. B, Beam Interact. Mater. Atoms 70 (1) (1992) 286–297, https://doi.org/10.1016/0168-583X(92)95944-M.

[21] C. Scheidenberger, H. Geissel, M. Maier, G. Münzenberg, M. Portillo, G. Savard, P. Van Duppen, H. Weick, M. Winkler, M. Yavor, F. Attallah, K.-H. Behr, V. Chichkine, S. Eliseev, M. Hausmann, M. Hellström, E. Kaza, B. Kindler, Y. Litvinov, B. Lommel, G. Marx, M. Matos, N. Nankov, T. Ohtsubo, K. Sümmerer, Z.-Y. Sun, Z. Zhou, Energy and range focusing of in-flight separated exotic nuclei – a study for the energy-buncher stage of the low-energy branch of the Super-FRS, in: 14th International Conference on Electromagnetic Isotope Separators and Techniques Related to Their Applications, Nucl. Instrum. Methods Phys. Res., Sect. B, Beam Interact. Mater. Atoms 204 (2003) 119–123, https://doi.org/10.1016/S0168-583X(02)01898-0.

[22] F. Greiner, T. Dickel, S. Ayet San Andrés, J. Bergmann, P. Constantin, J. Ebert, H. Geissel, E. Haettner, C. Hornung, I. Miskun, W. Lippert, I. Mardor, I. Moore, W.R. Plaß, S. Purushothaman, A.-K. Rink, M.P. Reiter, C. Scheidenberger, H. Weick, Removal of molecular contamination in low-energy ribs by the isolation-dissociation-isolation method, Nucl. Instrum. Methods Phys. Res., Sect. B, Beam Interact. Mater. Atoms 463 (2020) 324–326, https://doi.org/10.1016/j.nimb.2019.04.072.

[23] I. Mardor, S.A.S. Andrés, T. Dickel, D. Amanbayev, S. Beck, J. Bergmann, H. Geissel, L. Gröf, E. Haettner, C. Hornung, N. Kalantar-Nayestanaki, G. Kripko-Koncz, I. Miskun, A. Mollaebrahimi, W.R. Plaß, C. Scheidenberger, H. Weick, S. Bagchi, D.L. Balabanski, A.A. Bezbakh, Z. Brencic, O. Charviakova, V. Chudoba, P. Constantin, M. Dehghan, A.S. Fomichev, L.V. Grigorenko, O. Hall, M.N. Harakeh, J.-P. Hucka, A. Kankainen, O. Kiselev, R. Knöbel, D.A. Kostyleva, S.A. Krupko, N. Kurkova, N. Kuzminchuk, I. Mukha, I.A. Muzalevskii, D. Nichita, C. Nociforo, Z. Patyk, M. Pfützner, S. Pietri, S. Purushothaman, M.P. Reiter, H. Roesch, F. Schirru, P.G. Sharov, A. Spătaru, G. Stanic, A. State, Y.K. Tanaka, M. Vencelj, M.I. Yavor, J. Zhao, Mass measurements of As, Se, and Br nuclei, and their implication on the proton-neutron interaction strength toward the $N = Z$ line, Phys. Rev. C 103 (2021) 034319, https://doi.org/10.1103/PhysRevC.103.034319.

[24] C.J. Sofield, N.E.B. Cowern, J.M. Freeman, K. Parthasaradhi, Energy straggling of 5.486-MeV alpha particles in Al, Phys. Rev. A 15 (1977) 2221–2226, https://doi.org/10.1103/PhysRevA.15.2221.

[25] L. Varga, H. Wilsenach, O. Hall, T. Dickel, M. Reiter, D. Amanbayev, T. Davinson, D. Morrissey, I. Pohjalainen, N. Tortorelli, J. Yu, J. Zhao, S. Ayet, S. Beck, J. Bergmann, Z. Ge, H. Geissel, L. Heitz, C. Hornung, N. Kalantar-Nayestanaki, E. Khan, G. Kripko-Koncz, I. Mardor, M. Narang, W. Plass, C. Scheidenberger, M. Simonov, S. Singh, A. State, C. Theisen, M. Vandebrouck, P. Woods, Novel device to study double-alpha decay at the FRS Ion Catcher, Nucl. Instrum. Methods Phys. Res., Sect. A, Accel. Spectrom. Detect. Assoc. Equip. 1063 (2024) 169252, https://doi.org/10.1016/j.nima.2024.169252.

[26] I. Miskun, Commissioning, performance and possible applications of RFQ mass-filter in the diagnostic unit of the FRS Ion Catcher facility, Diploma thesis, 2015.

[27] F. Farinon, I. Kojouharov, C. Nociforo, S. Pietri, K.-H. Behr, A. Brunle, H. Geissel, C. Karagiannis, J. Kurcewicz, A. Prochazka, M. Ricciardi, C. Scheidenberger, Development and test of isomer tagging detector, GSI scientific report, 2009.

[28] F. Farinon, I. Kojouharov, C. Nociforo, S. Pietri, K.-H. Behr, A. Brunle, H. Geissel, C. Karagiannis, J. Kurcewicz, A. Prochazka, M. Ricciardi, C. Scheidenberger, Development and test of an α-tagger detector at the frs, GSI scientific report, 2011.
[29] C. Hornung, T. Dickel, D. Amanbayev, S. Ayet San Andrés, D.L. Balabanski, S. Beck, J. Bergmann, P. Constantin, J. Ebert, H. Geissel, F. Greiner, L. Gröf, E. Haettner, M.N. Harakeh, J.-P. Hucka, N. Kalantar-Nayestanaki, D.A. Kostyleva, G. Kripko-Koncz, I. Miskun, A. Mollaebrahimi, I. Mukha, G. Münzenberg, S. Pietri, W.R. Plaß, S. Purushotaman, M.P. Reiter, A.-K. Rink, H. Roesch, C. Scheidenberger, A. Spătaru, Y.K. Tanaka, H. Weick, J. Zhao, Mass tagging: verification and calibration of particle identification by high-resolution mass measurements, Nucl. Instrum. Methods Phys. Res., Sect. B, Beam Interact. Mater. Atoms 541 (2023) 257–259, https://doi.org/10.1016/j.nimb.2023.04.045.
[30] S. Purushothaman, S. Ayet San Andrés, J. Bergmann, T. Dickel, J. Ebert, H. Geissel, C. Hornung, W. Plaß, C. Rappold, C. Scheidenberger, Y. Tanaka, M. Yavor, Hyper-EMG: a new probability distribution function composed of Exponentially Modified Gaussian distributions to analyze asymmetric peak shapes in high-resolution time-of-flight mass spectrometry, Int. J. Mass Spectrom. 421 (2017) 245–254, https://doi.org/10.1016/j.ijms.2017.07.014.
[31] Evaluated nuclear structure data file, https://www.nndc.bnl.gov/ensdf/.
[32] M. Huyse, P. Dendooven, K. Deneffe, Production and mass separation of short-living neutron-deficient actinides, Nucl. Instrum. Methods Phys. Res., Sect. B, Beam Interact. Mater. Atoms 31 (3) (1988) 483–486, https://doi.org/10.1016/0168-583X(88)90350-3.
[33] E. Rey-herme, A. Raggio, M. Vandebrouck, I. Moore, I. Pohjalainen, C. Delafosse, R. de Groote, Z. Ge, S. Geldhof, M. Hukkanen, A. Kankainen, A. Koszorus, D. Nesterenko, J. Sarén, B. Sulignano, C. Theisen, D. Thisse, A.P. Weaver, Level structure of ^{221}Ac and ^{217}Fr from decay spectroscopy, and reflection asymmetry in ^{221}Ac, Phys. Rev. C 108 (2023) 014304, https://doi.org/10.1103/PhysRevC.108.014304.
[34] I. Miskun, T. Dickel, I. Mardor, C. Hornung, D. Amanbayev, S. Ayet San Andrés, J. Bergmann, J. Ebert, H. Geissel, M. Górska, F. Greiner, E. Haettner, W.R. Plaß, S. Purushothaman, C. Scheidenberger, A.-K. Rink, H. Weick, S. Bagchi, P. Constantin, S. Kaur, W. Lippert, B. Mei, I. Moore, J.-H. Otto, S. Pietri, I. Pohjalainen, A. Prochazka, C. Rappold, M.P. Reiter, Y.K. Tanaka, J.S. Winfield, F. the Super-FRS Experiment Collaboration, A novel method for the measurement of half-lives and decay branching ratios of exotic nuclei, Eur. Phys. J. A 55 (9) (2019) 148, https://doi.org/10.1140/epja/i2019-12837-8.
[35] A. El-Lawindy, J. Burrows, P. Butler, J. Cresswell, V. Holliday, G. Jones, R. Tanner, R. Wadsworth, D. Watson, K. Connell, J. Simpson, C. Lauterbach, J. Mines, Low-lying structure of ^{215}Rn and ^{219}Ra, J. Phys. G, Nucl. Phys. 13 (1999) 93, https://doi.org/10.1088/0305-4616/13/1/011.
[36] K. Valli, E.K. Hyde, J. Borggreen, Production and decay properties of thorium isotopes of mass 221-224 formed in heavy-ion reactions, Phys. Rev. C 1 (1970) 2115–2132, https://doi.org/10.1103/PhysRevC.1.2115.
[37] P.A. Tove, Alpha-emitters with short half-life induced by protons on heavy elements, Arkiv Fysik 13, https://www.osti.gov/biblio/4300480.
[38] A.R. Barnett, J.S. Lilley, Interaction of alpha particles in the lead region near the Coulomb barrier, Phys. Rev. C 9 (1974) 2010–2027, https://doi.org/10.1103/PhysRevC.9.2010.
[39] W.J. Ramler, J. Wing, D.J. Henderson, J.R. Huizenga, Excitation functions of bismuth and lead, Phys. Rev. 114 (1959) 154–162, https://doi.org/10.1103/PhysRev.114.154.
[40] H. Kudo, T. Nomura, K. Sueki, M. Magara, N. Yoshlda, Isomeric transitions of ^{211m}Po and ^{212m}Po and E4 effective charge, Nucl. Phys. A 494 (2) (1989) 203–213, https://doi.org/10.1016/0375-9474(89)90019-5.
[41] M. Bowry, Z. Podolyák, S. Pietri, J. Kurcewicz, M. Bunce, P.H. Regan, F. Farinon, H. Geissel, C. Nociforo, A. Prochazka, H. Weick, N. Al-Dahan, N. Alkhomashi, P.R.P. Allegro, J. Benlliure, G. Benzoni, P. Boutachkov, A.M. Bruce, A.M. Denis Bacelar, G.F. Farrelly, J. Gerl, M. Górska, A. Gottardo, J. Gręboszz, N. Gregor, R. Janik, R. Knöbel, I. Kojouharov, T. Kubo, N. Kurz, Y.A. Litvinov, E. Merchan, I. Mukha, F. Naqvi, B. Pfeiffer, M. Pfützner, W. Plaß, M. Pomorski, B. Riese, M.V. Ricciardi, K.-H. Schmidt, H. Schaffner, C. Scheidenberger, E.C. Simpson, B. Sitar, P. Spiller, J. Stadlmann, P. Strmen, B. Sun, I. Tanihata, S. Terashima, J.J. Valiente Dobón, J.S. Winfield, H.-J. Wollersheim, P.J. Woods, Population of high-spin isomeric states following fragmentation of ^{238}U, Phys. Rev. C 88 (2013) 024611, https://doi.org/10.1103/PhysRevC.88.024611.
[42] M. de Jong, A. Ignatyuk, K.-H. Schmidt, Angular momentum in peripheral fragmentation reactions, Nucl. Phys. A 613 (4) (1997) 435–444, https://doi.org/10.1016/S0375-9474(96)00460-5.
[43] A. Kelic, M.V. Ricciardi, K.-H. Schmidt, Towards a complete description of the decay channels of a nuclear system from spontaneous fission to multifragmentation, arXiv:0906.4193, 2009.
[44] J.-J. Gaimard, K.-H. Schmidt, A reexamination of the abrasion-ablation model for the description of the nuclear fragmentation reaction, Nucl. Phys. A 531 (3) (1991) 709–745, https://doi.org/10.1016/0375-9474(91)90748-U.
[45] Z. Podolyák, J. Gerl, M. Hellström, F. Becker, K. Gladnishki, M. Górska, A. Kelić, Y. Kopatch, S. Mandal, P. Regan, K.-H. Schmidt, P. Walker, H. Wollersheim, A. Banu, G. Benzoni, H. Boardman, E. Casarejos, J. Ekman, H. Geissel, H. Grawe, D. Hohn, I. Kojouharov, J. Leske, R. Lozeva, M. Mineva, G. Neyens, R. Page, C. Pearson, M. Portillo, D. Rudolph, N. Saito, H. Schaffner, D. Sohler, K. Sümmerer, J. Valiente-Dobón, C. Wheldon, H. Weick, M. Winkler, High angular momentum states populated in fragmentation reactions, Phys. Lett. B 632 (2) (2006) 203–206, https://doi.org/10.1016/j.physletb.2005.10.070.